Process parameter interaction effect on the evolving properties of laser metal deposited titanium for biomedical applications

Ezekiel Nyoni*& Esther T Akinlabi

Department of Mechanical Engineering Science

University of Johannesburg, South Africa

ABSTRACT

The laser power interaction effects on the evolving properties of commercially pure titanium during laser metal deposition were analysed. The optimized processing parameters obtained for this research study were, spot size of 4 mm, powder flow rate of 2 g/min, gas flow rate of 2 l/min, and the scanning speed set at 0.002m/s. A total of seven samples were fabricated by depositing titanium powder onto a Ti-6Al-4V base metal; using an Nd-Yag laser by varying the laser power from 400 to 1600 watts while keeping all the other parameters constant. The deposited samples were characterised through the evolving microstructure, microhardness, wear and the corrosion behaviour. The microstructural evaluation revealed that the ratio of dilution increased with an increase in the laser power. Furthermore, it was found that as the dilution increased, the wear resistance behaviour of the deposits decreased due to the increased foreign elements (Al and V) from the substrate which inhibited smooth fusion as the molten deposit cooled. Also, the microstructural evaluation showed that finer martensitic microstructures were obtained at lower laser power rating which was associated with inter-layer porosity and due to the low laser-material interaction. However, Widmanstätten structures were observed at higher laser power settings

* Corresponding Author – Email Address: e.nyoni@yahoo.com

together with the presence of intra-layer porosity which is desirable for osteointegration. For biocompatibility, immersion tests in the Hank's solution were conducted for 14 days. The atomic absorption spectroscopy analyses showed that no leaching happened during the immersion process for all the samples hence, confirming the desirable properties expected of biomedical implants. An overall overview on the effects of the laser power which has a significant effect on the evolving properties is essential in order to know how this process parameter can be controlled to attain certain properties of the material for specific and tailored functions.

Key words: Biocompatibility, Dilution, Laser Metal Deposition, Laser Power, Microstructure, Microhardness, Titanium, Wear resistance.

Introduction

Additive manufacturing (AM) is amongst the latest technologies being employed in the manufacturing industry for the production of a number of parts. Unlike olden days, the modern day consumers are requesting for more customized products than standardized ones [1, 2]. This has led to a greater demand in a manufacturing process that produces more customized goods in less manufacturing lead time [3, 4]. There are different types of additive manufacturing techniques and Laser Metal Deposition (LMD) is one of the techniques that are still being developed to meet bulk production standards in the flexible manufacturing industry.

Laser Metal Deposition (LMD) process uses Computer Aided Design (CAD) model and a laser beam source to fabricate the parts through layer by layer addition. In essence, the solid materials are delivered either in powder or wire form into a pool of molten material generated on a substrate by an incident laser beam. The powder materials melt and dissolve together with the molten substrate material. The laser beam is scanned over the surface of the substrate following a path generated from the produced CAD file. After which the molten materials solidify forming a deposited layer. For subsequent layers to follow, the same process is repeated [5].

Through LMD, complex shaped parts can be fabricated at ease and at low cost [6]. Most metals have their surfaces modified by the use of laser beams because of the high coherence and directionality of the beams [7]. Because of the poor machinability property of titanium, LMD is mostly used in the fabrication of titanium parts [7, 8]. LMD amongst other Laser Additive Manufacturing (LAM) methods is also used in the fabrication of a number of metal parts from the super alloys (e.g. titanium and nickel) to steels which are found in commonly made industrial goods. The Laser Additive Manufacturing methods are mostly preferred for the production of fully dense and near net-shaped parts which are difficult to produce using most additive manufacturing

methods [9]. Titanium and its alloys have been used in the aerospace and the medical fraternities for a while now because of their high strength light weight properties. However, the use of titanium and its alloys in the manufacturing industry is limited with the materials being hard to machine using conventional methods as they react with the tools at high temperatures causing massive tool wear. Also, with the repeatability problems experienced in the LMD processing of titanium, a lot of research interest has been developed in the laser metal deposition of titanium and its alloys for biomedical applications

Kobryn et al. [10] investigated the effect of the laser power and traverse speed on the microstructure, porosity, and build height in laser-deposited Ti-6Al-4V using a Laser Engineered Net Shaping (LENS) system. In their study, they discovered that high temperature gradients and high cooling gradients result in the formation of fine transformed and columnar microstructures. Also, they found out that the width of the columnar grains decreases with the increase in the cooling rates. They also noted that the laser power has no direct influence on the build height, however, they highlighted that porosity affect the solidification conditions of the deposit which in turn affect the build height.

A comparative study conducted by Wu et al. [11] on the microstructures of laser-deposited Ti-6Al-4V showed that the morphology of the deposited alloy is greatly influenced by directional heat extraction and a tendency of forming long columnar grains. It was observed that the length of the columnar grains decreased with an increase in the laser power and that large equiaxed grains were formed. The same phenomenon was observed by Shukla et al [12] at higher laser power setting of 3000 Watts. They attributed this to the fact that the temperature gradient reduces with the increase in the laser power. This is as a result of the fact that at higher laser power, more heat

is delivered to the substrate hence, the substrate remains hot for a longer period of time and therefore the decrease in the temperature gradient of the heat from the deposit to the substrate.

Brandl et al. [13] in their research work on the mechanical properties of additive manufactured titanium (Ti-6Al-4V) blocks deposited by a solid state-state laser and wire reported that a finer or equiaxed microstructure increases the strength and ductility whilst the lamellar microstructure reduces the strength and ductility. Brandl et al. [14, 15] did further studies on microstructural and mechanical properties of wire deposited Ti-6Al-4V using laser. In these studies they observed that the increase in the laser power resulted in the sizes of the grains in the melted and heat affected zones to increase. In these studies, they observed that the increase in the laser power resulted in the sizes for the grains in the melted and heat affected zones to increase. They also observed that the hardness of the deposited material increased with the increase in the laser power; as more substrate fused with the molten powders.

The same observation was reported by Mahamood et al. [6], whilst studying the effect of laser power on the microstructure and microhardness of the laser metal deposited Ti-6Al-4V. These studies attributed the impurities or alloying constituents from the substrate as the ones responsible for the increase in the hardness characteristics. Brandl et al. [16] attributed these findings to the post heat treatment that happens to the deposit, as more heat is delivered to the molten area. Then, there tends to be some work hardening effect as the molten deposit cools.

Oldani and Dominguez [17] discussed in detail the use of titanium as a biomaterial for implants. The problems they highlighted that hinder the use of titanium in the medical industry are that the cost of processing is too high, due to the difficulty in the machining of titanium. Hence, they suggested powder metallurgy as an alternative. Also, the other problem was that although the elastic modulus of titanium is relatively low compared to that of other metallic biomaterials in its

raw form, the elastic modulus of titanium is 4 to 6 times higher than that of the cortical bone. This causes stress shielding, and ultimately, the failure of the implants. Nonetheless, the solution to this problem can be reduced by controlling the porosity and morphology of the titanium during processing. The porosity of the titanium has to be controlled; because, if fully porous, the implant would not be able to sustain the physiological loads [17].

From the previous studies, it is imperative that some research work be done on titanium powder which is laser metal deposited onto a Ti-6Al-4V substrate, with the intention of producing a candidate material for biomedical application. For this research study, samples were fabricated by varying the laser power and keeping all the other operating parameters constant.

2. Experimental Technique

2.1 Fabrication of Samples

A preliminary study was first conducted to ascertain the process window for optimisation. These include the laser scanning speed, powder flow rate and gas flow rate. Preparation of the substrate was done by sandblasting it using a guyson sand blaster and cleaned with acetone to remove the dirt. This was done to remove foreign particles on the surface of the substrate and also to increase the adsorption capacity of the substrate.

The fabrication of the samples was done using a Kuka robot to deliver a 4.4 kW Nd-YAG laser. Also on the robot end effector, was a coaxial nozzle which was used to deliver the powder onto the melt pool as shown in Figure 1. Argon gas was used as a delivery mechanism for the powder which was used as a shielding gas for the powder as well. Also, a plastic cover box was used to cover the deposition platform in order to prevent oxidation from taking place during the deposition. From the results of the deposited samples in the preliminary study, final processing parameters were chosen which are shown in Table I.

<insert Figure1>

<insert Table I >

The Laser Energy Density is described as the laser energy available on a specific area of concern for a specific amount of time. Hence, it is mainly affected by the laser spot size which has an effect on the focused area and the laser scanning speed which determines the amount of time the laser is focused on that area [18].

The Laser energy density (LED) was calculated using Equation 1

$$LED = \frac{Laser\ power\ (KW)}{Spot\ size(m) \times Scanning\ Speed\ (\frac{m}{s})} \qquad (1)$$

From Equation 1, it can be seen that the smaller the spot, the higher the LED. Mahamood et al. [18] maintained that the smaller the spot size, the higher the LED available to melt the powder. This is mainly because the laser power becomes more energy intensive, as the laser energy available is concentrated on a smaller area. This improves the material efficiency; as there is more powder melted, because of the higher LED.

2.2 Material Characterisation

Metallurgical preparation and characterization of the deposited samples

The samples for microstructural characterizations were cut into 10 mm lengths. The sample preparation was conducted according to the ASTM E3-11 standard guide for preparation of metallographic specimens and the application notes from Struers for the metallographic preparation of titanium [19, 20]. The sample preparation for microscopy included cutting off 10 mm in length samples from each deposit. They were then mounted, grinded and polished according to the ASTM E3-11 standard. Before the samples could be viewed under an optical microscope,

they were etched using the Kroll's reagent. The same procedure without the etching part was followed for the samples on which a feasible microhardness study was done.

The microscopy of the etched samples was first done under an Olympus BX51M optical microscope to characterize the zones. In addition to view and characterize the microscopic zones of the samples, the dimensions of the different properties of these microscopic zones were also measured under the microscope using the stream essentials software. The same software was used to estimate the porosity on the samples. Also, for further accuracy and characterization of the morphology of the samples, microscopy was also done using a Tescan Scanning Electron Microscope (SEM). The hardness test was done, according to the ASTM E384-11 standard [21]. The EMCO hardness tester was used. The indenter chosen was a diamond indenter; and the indentations were done two per zone in the cross section at a spacing of 0.1 mm with 15 seconds dwelling time for a 500gf.

2.3 Estimation of the Deposit and the Dilution Areas

To characterize how the deposit and dilution zones related to the change in the laser power during the deposition, the deposit and the dilution zones had to be calculated. The two zones were circular sectors, Figure 2 and Equation 3 show how the areas of the deposition zone together with the dilution zone area were estimated.

<insert Figure 2 >

The circular sector area to be calculated is as shown in the Figure 2 with the boundaries of the sector being the arc s and the chord A.

$A = A_{sector} - A_{isosceles\ triangle}$ (2) =

$\frac{R^2}{2}(\theta - sin\,\theta)$

$= R^2\,cos^{-1}\left(\frac{r}{R}\right) - r\sqrt{(R^2 - r^2)}$ *but r = R-h therefore*

$= R^2\,cos^{-1}\left(\frac{R-h}{R}\right) - (R-h)\sqrt{(R^2 - (R-h)^2)}$ (3) [22] (3)

This formula was employed at a later stage to estimate the deposit and the dilution areas of the samples produced.

<insert Figure 3 >

The dilution % was then calculated using Equation 4 by incorporating areas estimated using Equation 3.

$$D = \frac{A_M}{A_D + A_M} \times 100 \quad [23] \qquad (4)$$

D - Dilution Percentage

A_M – Area of the melted zone

A_D – Area of the deposited zone

2.4 Wear Testing

The dry ball sliding test was done to test the tribological wear properties of the deposits. The test was done according to ASTM G133 – 05 (2010) standard [24]. The tests were performed using a UMT 2CETR tribotester with a ball-on-plate arrangement. A load of 25 N with a stroke length of

2 mm was applied to the Tungsten Carbide ball of 10mm in diameter, the ball was allowed to slide onto the tracks at a reciprocating frequency of 20Hz for a sliding time of 1000s.

Estimation of wear volume

The wear surfaces were analyzed further under a scanning electron microscope, where the wear scar dimensions were taken. Due to the skewness of the wear tracks, three measurements were taken for each wear track; and the average was then used for the calculations. The dimensions are as shown in Figure 4. From the information gathered from the tribometer during the wear test, the graphs of the wear volume were drawn. All the results were illustrated and discussed in the successive sections.

<insert Figure 4 >

The wear volume was then calculated using Equation 5, which was suggested by Sharma et al. [25]. Using the wear volume, all the calculations were determined in Microsoft Excel.

$$V_w = L\left[r^2\sin^{-1}\left(\frac{w}{2r}\right) - \frac{w}{2}\left(r^2 - \frac{w^2}{4}\right)^{1/2}\right] + \frac{\pi}{3}\left[2r^3 - 2r^2\left(r^2 - \frac{w^2}{4}\right)^{1/2} - \frac{w^2}{4}\left(r^2 - \frac{w^2}{4}\right)^{1/2}\right] \quad (5)$$

Where;

V_w = Wear volume in mm^3

L = Stroke length mm.

r = Ball radius in mm.

w = Wear track width.

2.5 Biocompatibility

One of the main objectives of this study was to assess the in vitro biocompatibility capacity of the titanium deposits since the samples are mainly used in the medical industry for different medical implants. The immersion tests were done in this study using the Hank's solution as the simulated body fluid. SEM analysis was done on the samples before they were placed in seven different beakers, whereupon an amount of 30 ml of Hanks solution was poured into the beakers. The beakers were then wrapped in wrapping plastics, before they were placed in an automatic water bath system that had the temperature kept at a constant of 37.5˚C ± 1 ˚C. Initially, the immersion was done for 2 hours; and a SEM analysis was done on them again; and a SEM was done after 5 hours; and lastly after 14 days. The specimens were immersed in the Hank's solution with the deposited surfaces facing down, to ensure that all the leached material would fall into the solution, thereby avoiding the leached material sticking onto the surfaces of the samples if they were immersed facing upwards. An Atomic Absorption Spectroscopy was done on the Hank's solution to check the amount of titanium that had leached into the solution.

3. Results and discussion

3.1 Microstructural Analysis

The microstructural changes that took place for the different deposits with the variation of the laser power were observed under an optical microscope. The dimensions of the respective zones were measured for all the deposited samples. The variation of the dimensional properties of the deposited and the melted zones with respect to the change in the laser power are shown in Figure 5.

<insert Figure5>

The length and the height of the HAZ increased as more energy was absorbed into the substrate, it sank deeper and wider into the substrate. However, there was a decrease in the height of the deposit simply because as the laser power increased, more of the substrate were melted and the fusion of the melted powder and the substrate started to take place deeper within the substrate than at the surface.

The ultimate dilution ratio to the respective laser power setting employed for the particular deposits has the variation shown in Figure 6.

<insert Figure 6 >

The LED was calculated using Equation 1 and with all the processing parameters except the laser power kept constant, the LED increased with an increase in the laser power as they are directly proportional. As illustrated in Figure 6, the increase in the Laser Energy Density led to the increase in the dilution rate. The dilution rate went up from 0% at 400 Watts to 68.7% at 1600 Watts. The increase in the dilution rate led to an increase in the fusion area as more substrate melted to fuse with the molten powder particles. The dilution area which is also termed as the fusion zone in this document also increased with an increase in the LED as it is directly proportional to the dilution ratio. This is in confirmation with the findings of Mansur et al. [26].

As described earlier, finer martensitic microstructures were obtained at lower laser power rating. This was because at low laser power, the melt pool was small enough for rapid solidification. As Mahamood et al. [27] illustrated that at high cooling rates, the microstructure of the deposits is more martensitic. However, with an increase in the laser power, the melt pool gets wider which

takes a long time to solidify, the slow cooling rates result in more coarse Widmanstätten structures being obtained. These microstructural variations are illustrated in Figure 7.

<insert Figure 7 >

The variation of the microstructure properties with an increase in the laser power is also seen on the intensity of the porosity and particle inclusions. The porosity variation is as shown in Figure 8. Initial increase in the laser power resulted in a decrease in the interlayer porosity whilst the intralayer porosity increases. This was mainly because more of the substrate began to melt hence, the porosity at the fusion boundaries decreased. However, at moderate laser power settings, intralayer porosity was relatively high owing to the particle inclusions caused by powder granules that were not fully melted as well as trapped gas bubbles. After further increase in the laser power, it was observed that more of the powder were melted and also the slow cooling rates provided a platform for all the trapped gases to vaporize hence, the reduction in the degree of porosity.

<insert Figure 8 >

3.2 Microhardness Profiling

The Vickers microhardness profiling was conducted on all the deposited areas for all the samples by avoiding porosity, and also as on the pure titanium parent material. The hardness values that were achieved are shown in Figure 9. The general trend was that the microhardness values increased with an increase in the laser power. At the lowest power rating of 400 Watts employed, the hardness value was 174.2 HV, which was a little less than that of the parent material with a value of 175.2 HV. The low microhardness result at low laser power can be attributed to the unmelted powders caused by high cooling rates at a low melt pool size. However, as the laser

power increased to a moderate power of 1000 Watts, the microhardness increased as well, with the hardness value of 298.83 at 1000 Watts. The sharp increase in the hardness value above the hardness of the parent material is because of the martensitic structure that forms within this power range. However, as the microstructure changes to a more Widmanstätten structure, the microhardness also increases slightly. However, the average grain size increases with increases in laser power, and with the hardness increasing. As explained earlier, for the samples produced with more laser power, the melt pool increases in size and the cooling rate reduces. Hence, the outside cools faster than the inside. This phenomenon results in the deposit cooling first, and then the fusion zone, and lastly, the HAZ. The difference in the cooling results in the work hardening of the top surfaces of the deposit and the fusion zone.

<insert Figure 9 >

3.3 Wear Behaviour Analysis

The wear behaviour of a material is affected by the inherent microstructure and hardness of the material; hence the previous findings on the microstructure and the hardness were correlated to the wear behaviour of the deposited samples in the following subsections.

Wear track characterization

The track width behaviour as the laser power is increased is shown in Figure 10. The widest wear track was observed on the sample produced at 1600 Watts with a width of 1.64 mm.

<insert Figure 10 >

From the morphologies shown, it was observed that wear by pitting increased as the laser power increased from 400 Watts to 800 Watts. However, pitting decreased with an increase in the laser

power from 1000 Watts to 1600 Watts. Some of the pitting along the wear tracks was as a result of surface fatigue caused by the sliding ball. However, pitting due to surface fatigue, reduced with increase in laser power, because of the increase in the surface hardness. Figure 11 shows the ploughing, grooving and pitting that took place during the wear sliding tests.

<insert Figure 11 >

Ploughing and grooving were apparent on all the samples, but were minimal on the samples produced at lower laser power of 800 Watts and below where the pitting was greatest. As explained by Bansal et al. [28], less ploughing and grooving suggests the propensity of body abrasive wear. The increase in the intensity of ploughing and grooving shows the increase of more plastic deformation behaviour, with an increase in the laser power with less abrasive wear modes. The relative increase in the plastic deformation behaviour with an increase in the laser power can be regarded as caused by the smooth surfaces obtained at higher laser power settings, which were as a result of complete melting of the deposited powder particles.

Wear Volume

Figure 12 shows how the wear volume varied with the increase in the laser power during the course of these experiments. Generally, the wear volume increased with an increase in the laser power. This can be ascribed to the fact that with the increase in the laser power, it was observed that the microstructure evolved from less martensitic to a more Widmanstätten structure, which is less compact. As the laser power increased, the wear volume increased as well. However, the slope of increase is higher as the laser power decreases. The wear scar volume of the CP Ti, which was the control material was 0.076 mm^3 with the least wear volume on the deposited tracks at 600 Watts,

with a wear volume of 0.061 mm^3. The largest wear volume was found in samples produced at 1600 Watts; and the maximum laser power setting was obtained with a wear volume of 0.24 mm^3. Generally, the wear volume increased with an increase in the laser power. This can be ascribed to the fact that with the increase in the laser power, it was observed that the microstructure evolved from less martensitic to a more Widmanstätten structure, which is less compact. As the laser power increased, the wear volume increased as well. However, the slope of increase is higher as the laser power decreases. The wear scar volume of the CP Ti, which was the control material was 0.076 mm^3 with the least wear volume on the deposited tracks at 600 Watts, with a wear volume of 0.061 mm^3. The largest wear volume was at 1600 Watts; and the maximum laser power setting was obtained with a wear volume of 0.24 mm^3.

<insert Figure 12 >

The increase in both the wear volume and the wear scar width generally depicts a decrease in the wear resistance. As explained by Moosa et al. [29], dilution has substantial effects on the bond strength of the deposited layers, especially for bond strength sensitive applications that require good wear resistance. However, there is a specific limit to which the dilution area should be increased, in order for a better wear resistant surface to be achieved. After which, any increase in the dilution rate conceives poor wear resistance surfaces. Hence, from this investigation, the drop in the wear volume between the 600 and 800 Watts determines the range where the wear resistance was at a maximum, with a dilution percentage of between 9.5% to 28.5%. Furthermore, an increase in the dilution after the dilution resulted in a drop in the wear resistance.

3.4 Biocompatibility Analysis

The biocompatibility analysis of the samples deposited at 400 Watts laser power are presented in Figures 13 (a) to (c). The Figures show the SEM images of the morphology of the samples before the immersion, after 5 hours, and after 14 days of immersion in Hank's solution.

<insert Figure 13 >

As shown from Figures 13 (a) to (c), the morphology became lighter or pale in colour; whereas before immersion, it was a bit darker in colour. As explained by Geetha et al. [30] and Balla et al. [31], the interaction of the Hank's solution and the oxide layer on top of the deposit, which was formed soon after the LMD process. Hence, this depassivation caused the difference in the colour contrast. White flakes were also noticed and on the surfaces of the granules on the deposit, together with white inclusions. All the other samples that were deposited at different laser power settings showed the same variation for the given immersion period as the 400 Watts sample. Therefore, an atomic absorption spectroscopy was done on the simulated body fluid.

Atomic Absorption Spectroscopy analyses of the immersion solutions

An Atomic Absorption Spectroscopy analysis was conducted to check the leaching of the titanium into the Hank's solution after two weeks of the immersion of the deposits into the Simulated Body Fluid. Figure 14 shows the leaching concentration of the deposited titanium into the Hank's solution after 14 days.

<insert Figure 14 >

Generally, the concentrations found in the Hank's solutions after two weeks were very much low. From Figure 14, it can be noted that there was no great variation in these concentrations; as

all were within the range of 0.002 mg/l to 0.005 mg/l where most had titanium concentrations of 0.005 mg/l. This was expected; as the titanium is considered to be a bioinert material under the given conditions.

4 Conclusions

The interaction effects of the processing parameters and the evolving properties of laser metal deposited titanium tailored for biomedical implants were successfully achieved in this study.

1. From the macrostructural observations, the deposit widths of the samples and the width HAZ widened with an increase in the laser power. As expected, these observations were attributed to the increase in the Laser Energy Density (LED), which increased the dilution rate for the laser interaction time. For the processing parameter window that was used in this research study, the maximum dilution ratio achieved was 68% at a power rating of 1600 Watts, which can be considered as the optimum setting obtained from this study.

2. The Energy Dispersive Spectroscopy analysis conducted on the deposited samples confirmed the increase in the dilution ratio; as more Vanadium and Aluminium elements that were previously in the substrate showed a substantial increase in the fusion zone with the increase in the laser power. Hence, to achieve a more dilute mixture of the substrate and the powder, the increase of the laser power is essential.

3. It was also observed that at low laser power settings, the martensitic structures were to be expected; as the cooling rates were high; while the Widmanstätten structures were observed at higher laser power; as the cooling rates were slower. This trend was also observed in this research study, as the laser power was increased. Sugahara et al. [32] showed that the more

the microstructures are Widmanstätten, the more oxidation and creep resistant they would become. Hence, for components to be used in conditions in which the temperatures will be very high, it is advised that higher laser power be used to achieve finer Widmanstätten structures – with better oxidation and creep resistance properties. However, for biomedical applications, this is not relevant; as the bone implants would only be exposed to temperatures within the range of body temperatures.

4. There was a general increasing trend in the hardness values, with an increase in the laser power; however, no metallurgical notch was formed. This can be attributed to the work hardening of the surface of the coating that has taken place during the cooling phase of the process. The increase in the hardness that could have resulted due to oxidation was disregarded in this study; as the argon gas and a plastic cover box were used for shielding, to provide an oxygen inert environment during the deposition process.

5. There was a general decrease in the wear resistance behaviour of the deposits; as the laser power increased. As mentioned earlier, the dilution ratio has a major effect on the bond strength of the solidified melt pool. The increase in the dilution ratio decreased the bond strength gradually, hence resulting in the decrease in the wear resistance behaviour, as confirmed by the increase in the wear volume. This behaviour can be attributed to the increase of the aluminium and vanadium elements in the fusion zone; as these alloying elements distort the bonding strength of the titanium; since they act as impurities.

Acknowledgments

The authors would like to acknowledge the support offered by the University of Johannesburg Mechanical Engineering Science Department and the Council of Scientific and Industrial Research (CSIR) National Laser Centre, Pretoria, South Africa.

References

[1] D. L. Bourell, J. J. J. Beaman, M. C. Leu and D. W. Rosen, “A Brief History of Additive Manufacturing and the 2009 Roadmap for Additive Manufacturing: Looking Back and Looking Ahead,” in RapidTech 2009: US-TURKEY Workshop on Rapid Technologies, Instabul, 2009.

[2] C. W. Fink, “An Overview of Additive Manufacturing, Part II,” Advanced Material, Manufacturing and Testing Information Analysis Center (AMMTIAC) Quarterly, vol. 4, no. 3, pp. 7-10, 2009.

[3] R. M. Mahamood, E. T. AkinlabiI, M. Shukla and S. Pityana, “Revolutionary Additive Manufacturing : An Overview,” in Lasers in Engineering, Old City Publishing, 2014, pp. 161-178.

[4] C. W. Fink, “An Overview of Additive Manufacturing, Part I,” Advanced Material, Manufacturing and Testing Information Analysis Center (AMMTIAC) Quarterly, vol. 4, no. 2, pp. 9-12, 2009.

[5] O. F. Ochonogor, C. Meacock, S. L. Pityana, P. A. I. Popoola and D. J. Majumder, “Microstructure characterization of laser-deposited titanium carbide and zirconium-based titanium metal matrix composites,” Journal of the Southern African Institute of Mining and Metallurgy, vol. 112, no. 10, 2012.

[6] R. M. Mahamood, E. T. Akinlabi, M. Shukla and S. Pityana, “Laser Metal Deposition of Ti6Al4V : A Study on the Effect of Laser Power on Microstructure and Microhardness,” in Proceedings of the International MultiConference of Engineers and Computer Scientists, Hong Kong, 2013.

[7] Y. S. Tian, C. Z. Chen, S. T. Li and Q. H. Huo, “Research progress on laser surface modification of titanium alloys,” Applied Surface Science, vol. 242, pp. 177-184, 2005.

[8] N. Dalili, A. Edrisya, K. Farokhzadeha, J. Lib, J. Lob and A. R. Riahia, “Improving the wear resistance of Ti–6Al–4V/TiC composites,” Wear, vol. 269, pp. 590-691, 2010.

[9] Y.-H. Pan, Part Height Control of Laser Metal Additive Manufacturing Process, Missouri Uiversity Of Science And Technology, 2013.

[10] P. A. Kobryn, E. H. Moore and S. S. L, “The Effect of Laser Power and Transverse Speed on Microstructure, Porosity, and Built Height in Laser-Deposited Ti-6Al-4V,” Scripta Materialia, no. 43, pp. 299-305, 2000.

[11] X. Wu, J. Liang, J. Mei, C. Mitchell, P. S. Godwin and W. Voice, “Microstructures of laser-deposited Ti–6Al–4V,” Materials and Design, no. 25, pp. 137-144, 2004.

[12] M. Shukla, R. M. Mahamood, E. T. Akinlabi and S. Pityana, “Effect of Laser Power and Powder Flow Rate on Properties of Laser Metal Deposited Ti6Al4V,” International Journal of Mechanical, Industrial Science and Engineering Vol:6 No:11, 2012, vol. 6, no. 11, pp. 35-39, 2012.

[13] E. Brandl, F. Palm, V. Michilov, B. Viehweger and C. Leyens, “Mechanical properties of additive manufactured titanium (Ti-6Al-4V) blocks by a solid-state laser and wire,” Materials and Design, no. 32, pp. 4665-4675, 2011.

[14] E. Brandl, V. Michailov, B. Viehweger and C. Leyens, “Deposition of Ti–6Al–4V using laser and wire, part I: Microstructural properties of single beads,” Surface & Coatings Technology, no. 206, p. 1120–1129, 2011.

[15] E. Brandl, V. Michailov, B. Viehweger and C. Leyens, “Deposition of Ti-6Al-4V using laser and wire, part II: Hardness and dimensions of single beads,” Surface & Coatings Technology , no. 206, pp. 1130-1141, 2011.

[16] E. Brandl, A. Schoberth and C. Leyens, “Morphology, microstructure, and hardness of titatnium (Ti-6Al-4V) blocks deposited by wire-feed additive layer manufacturing (ALM),” Materials and Science Engineering A, no. 532, pp. 295-307, 2012.

[17] C. Oldani and A. Dominguez, “Titanium as a Biomaterial for Implants,” in Recent Advances in Arthroplasty, pp. 149-163.

[18] R. M. Mahamood, E. T. Akinlabi, M. Shukla and S. Pityana, “Improving Surface Integrity using Laser Metal Deposition Process,” in Surface Engineering Techniques and Applications: Research Advancements, IGI Global, 2014, pp. 146-176.

[19] ASTM International, (E3-11) Standard Guide for Preparation of Metallographic Specimens, ASTM International, 2011.

[20] Struers, Metallographic preparation of titanium, Struers, 2008.

[21] ASTM International, (E384-11) Standard Test Method for Knoop and Vickers Hardness of Materials, ASTM , 2012.

[22] E. W. Weisstein, “Wolfram Mathworld,” MathWorld, [Online]. Available: http://mathworld.wolfram.com/CircularSegment.html. [Accessed 28 November 2014].

[23] S. D. Sun, Q. Liu, M. Brandt, M. Janardhana and G. Clark, “Microstructure and mechanical properties of laser cladding repair of AISI 4340 Steel,” in 28th International congress of aeronautical sciences, 2012.

[24] ASTM International, (G133-05) Standard Test Method For Linearly Reciprocating Ball-on-Flat Sliding Wear, ASTM International, 2010.

[25] S. Sharma, S. Sangal and K. Mondal, “On the optical microscopic method for the determination of ball-on-flat surface linearly reciprocating sliding wear volume,” Wear, no. 300, pp. 82-89, 2013.

[26] M. R. Mansur, J. Wang and C. C. Berndt, “Microstructure, composition and hardness of laser-assisted hydroxyapatite and Ti-6Al-4V composite coatings,” Surface & Coatings Technology, vol. 232, pp. 485-488, 2013.

[27] R. M. Mahamood, E. T. Akinlabi, M. Shukla and S. Pityana, “Characterizing the Effect of Laser Power Density on Microstructure, Microhardness, and Surface Finish of Laser Deposited Titanium Alloy,” Journal of Manufacturing Science and Engineering , vol. 135, no. 6, 2013.

[28] D. G. Bansal, O. L. Eryilmaz and P. J. Blau, “Surface engineering to improve durability and lubricity of Ti-6Al-4V alloy,” Wear, no. 271, pp. 2006-2011, 2011.

[29] A. A. Moosa, M. J. Kadhim and A. D. Subh, “Dilution Effect during Laser Cladding of Inconel 617 with Ni-Al powders,” Modern Applied Science Vol. 5, No. 1; February 2011 , vol. 5, no. 1, pp. 50-55, 2011.

[30] M. Geetha, D. Durgalakshmi and R. Asokamani, “Biomedical Implants: Corosion and its Prevention - A Review,” Recent Patents on Corrosion Science , vol. 2, pp. 40-54, 2010.

[31] V. K. Balla, M. Das, S. Bose, J. G. D. Ram and I. Manna, “Laser surface modification of 316 L stainless steel with bioactive hydroxyapatite,” Materials Science and Engineering C, no. 33, pp. 4594-4598, 2013.

[32] T. Suguhara, D. A. P. Reis, C. Moura Neto, M. J. R. Barboza, E. A. C. Perez, F. Piorino Neto and A. C. O. Hirschmann, “The Effect of Widmanstatten and Equiaxed Microstuctres of Ti-6Al-4V on the Oxidation Rate and Creep Behaviour,” Material Science Forum, Vols. 636-637, pp. 657-662, 2010.

Table I : Laser Metal Deposition matrix

Sample	Laser power (watts)	Powder flow rate g/min	Gas flow rate l/min	Scanning Speed m/s	Spot size mm
1	400	2	2	0.002	4
2	600	2	2	0.002	4
3	800	2	2	0.002	4
4	1000	2	2	0.002	4
5	1200	2	2	0.002	4
6	1400	2	2	0.002	4
7	1600	2	2	0.002	4

List of Figure Captions

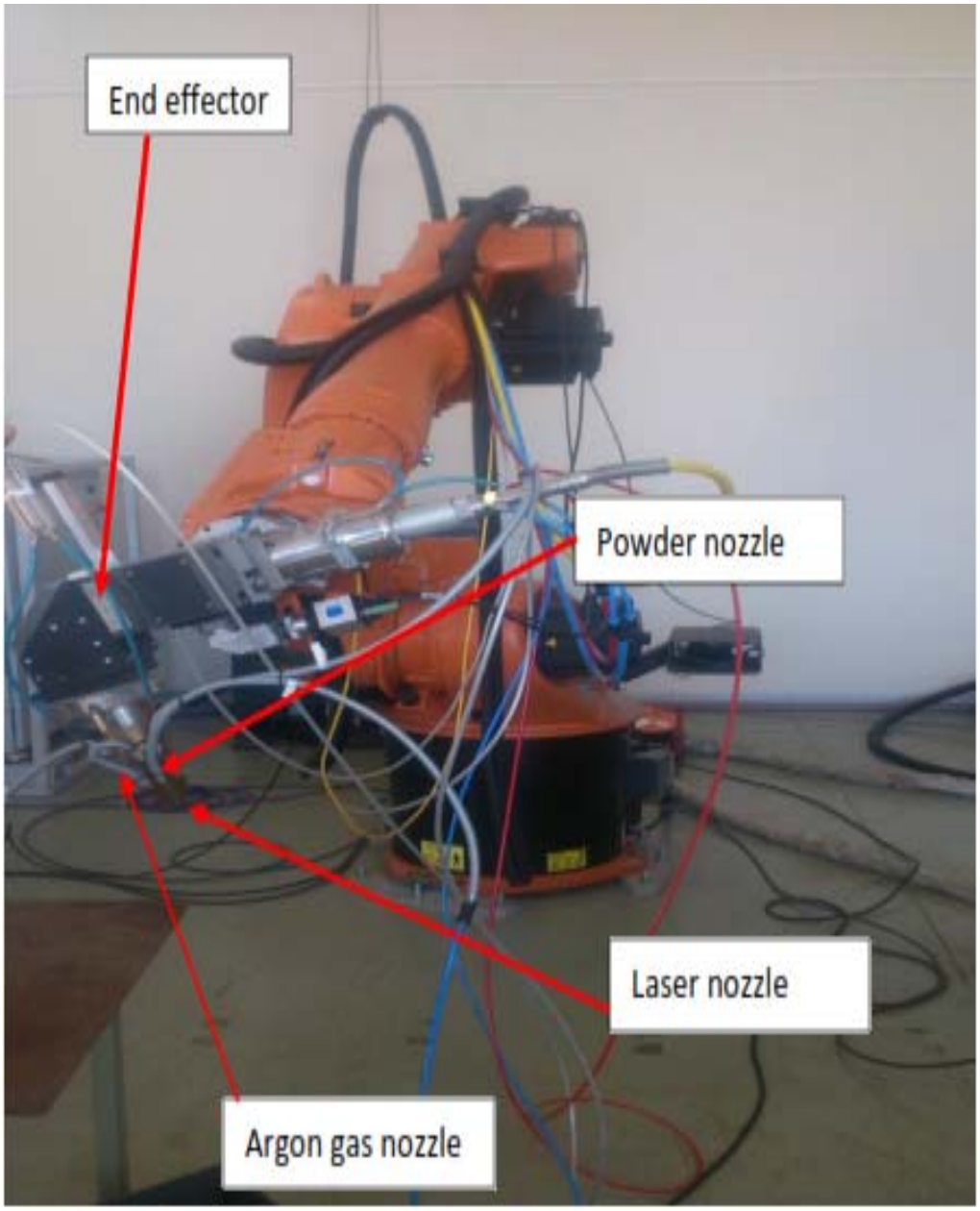

Figure 1

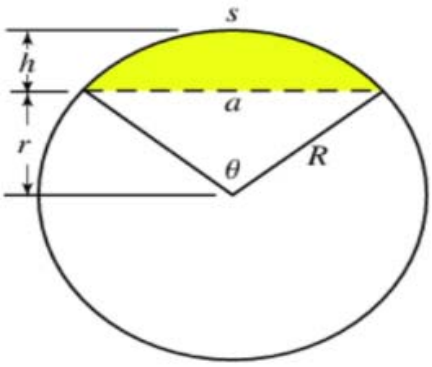

Figure 2

Figure 3

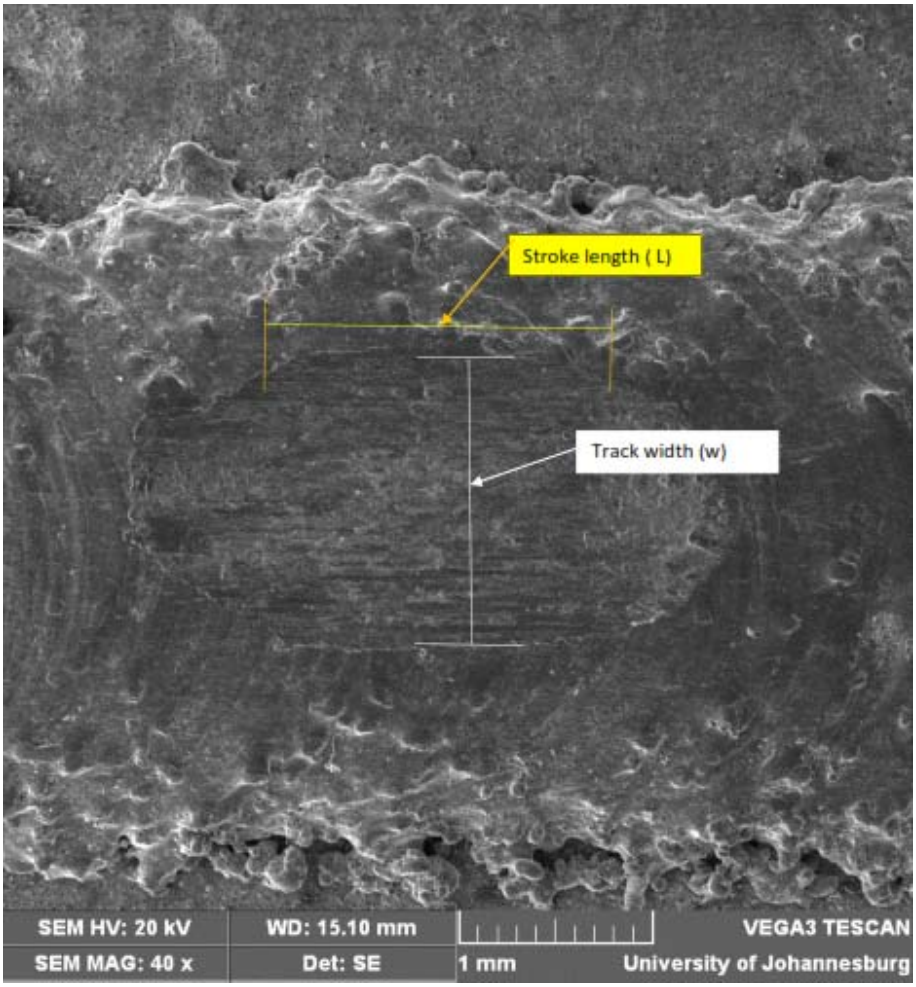
Stroke length (L)
Track width (w)
SEM HV: 20 kV
WD: 15.10 mm
VEGA3 TESCAN
SEM MAG: 40 x
Det: SE
1 mm
University of Johannesburg

Figure 4

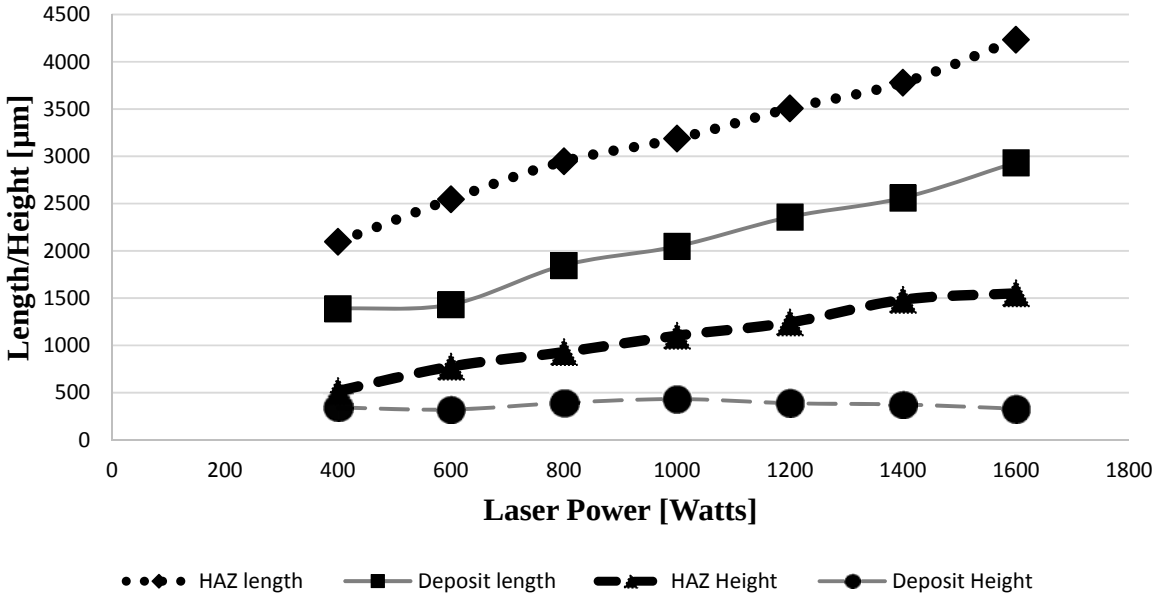

Figure 5

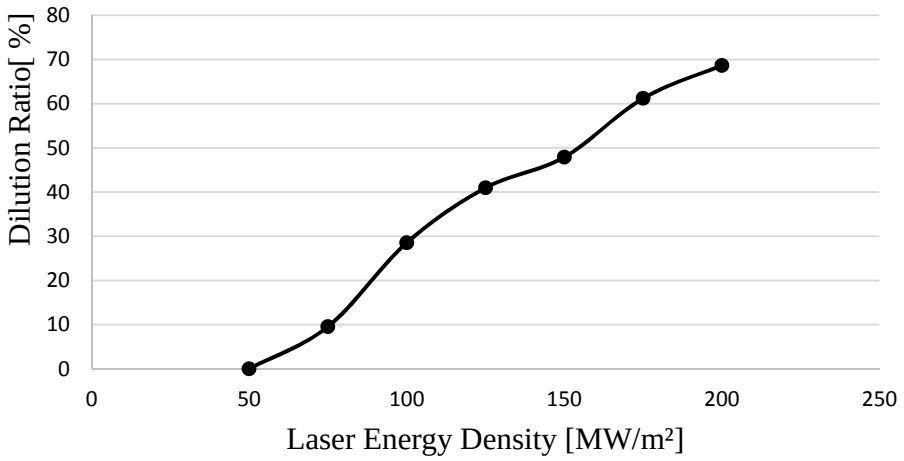

Figure 6

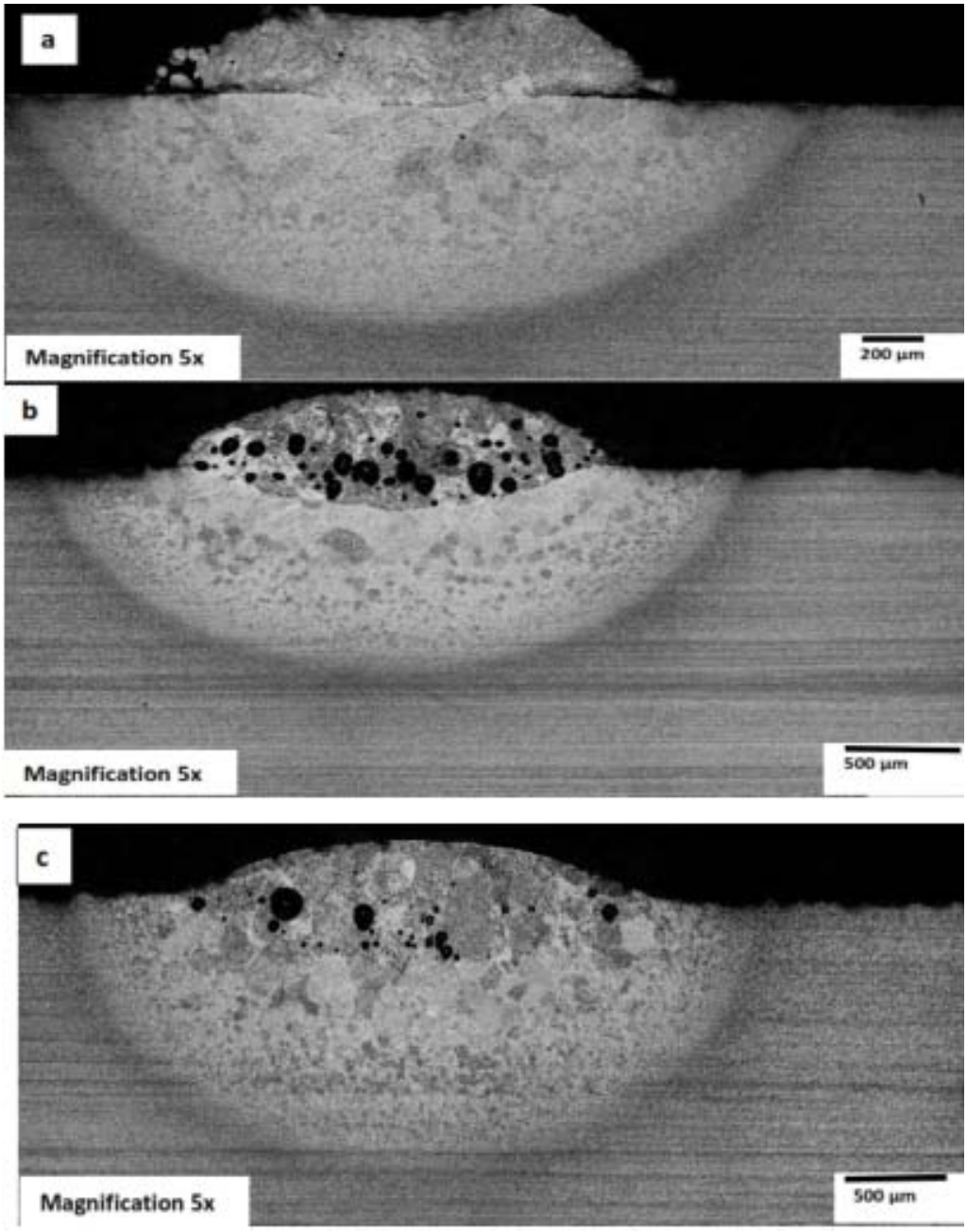
a
Magnification 5x
200 µm
b
Magnification 5x
500 µm
c
Magnification 5x
500 µm

Figure 7

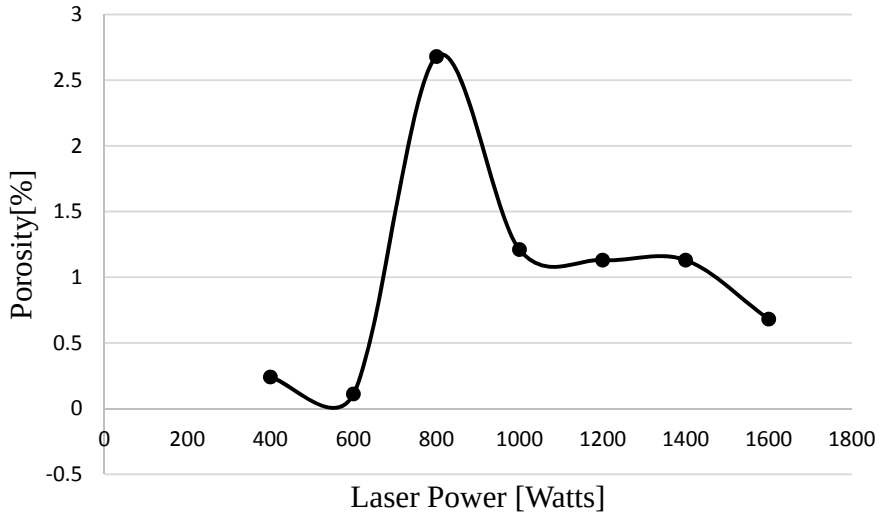

Figure 8

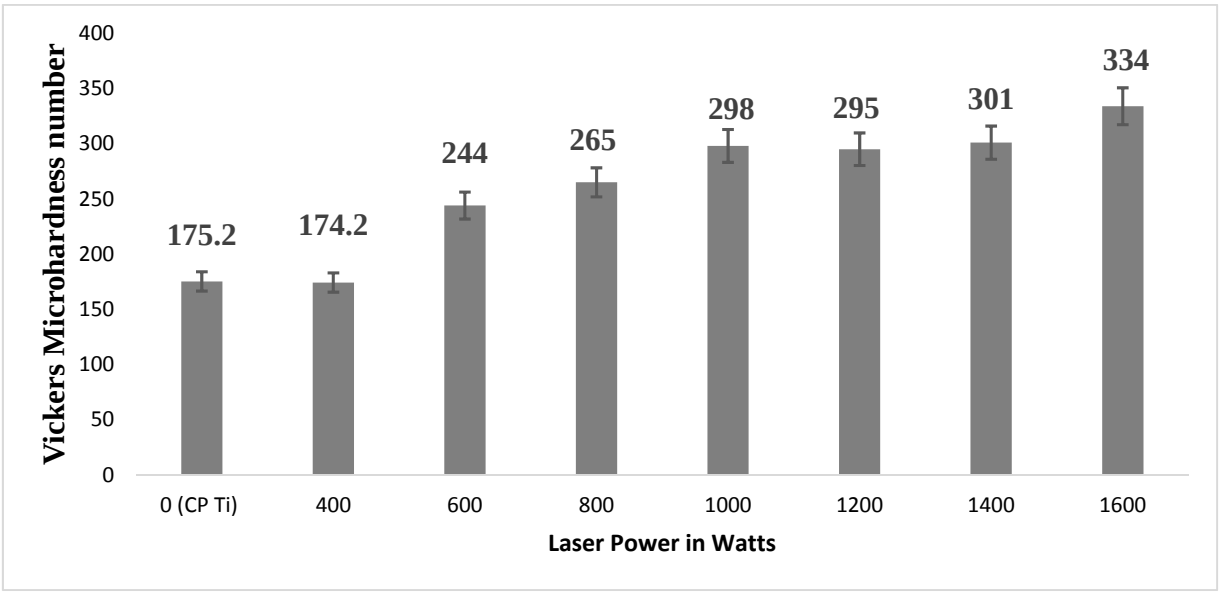

Figure 9

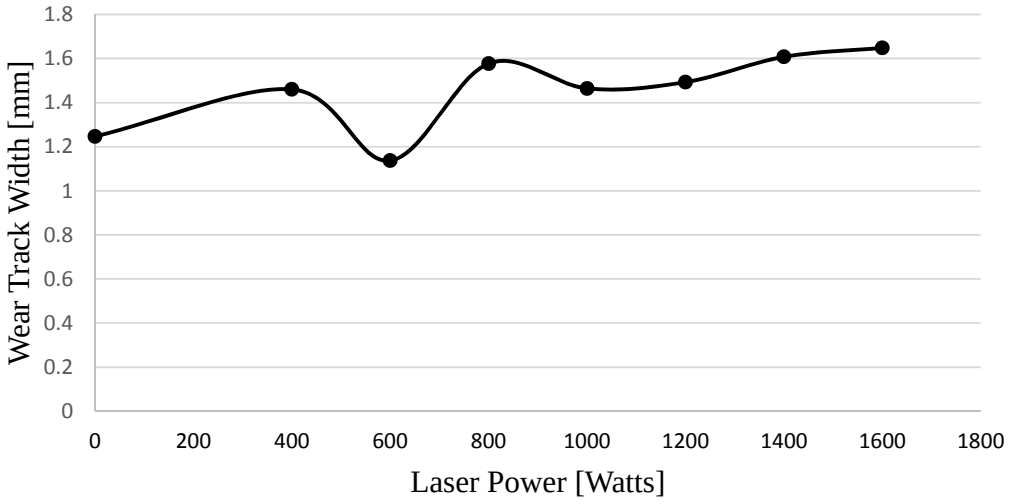

Figure10

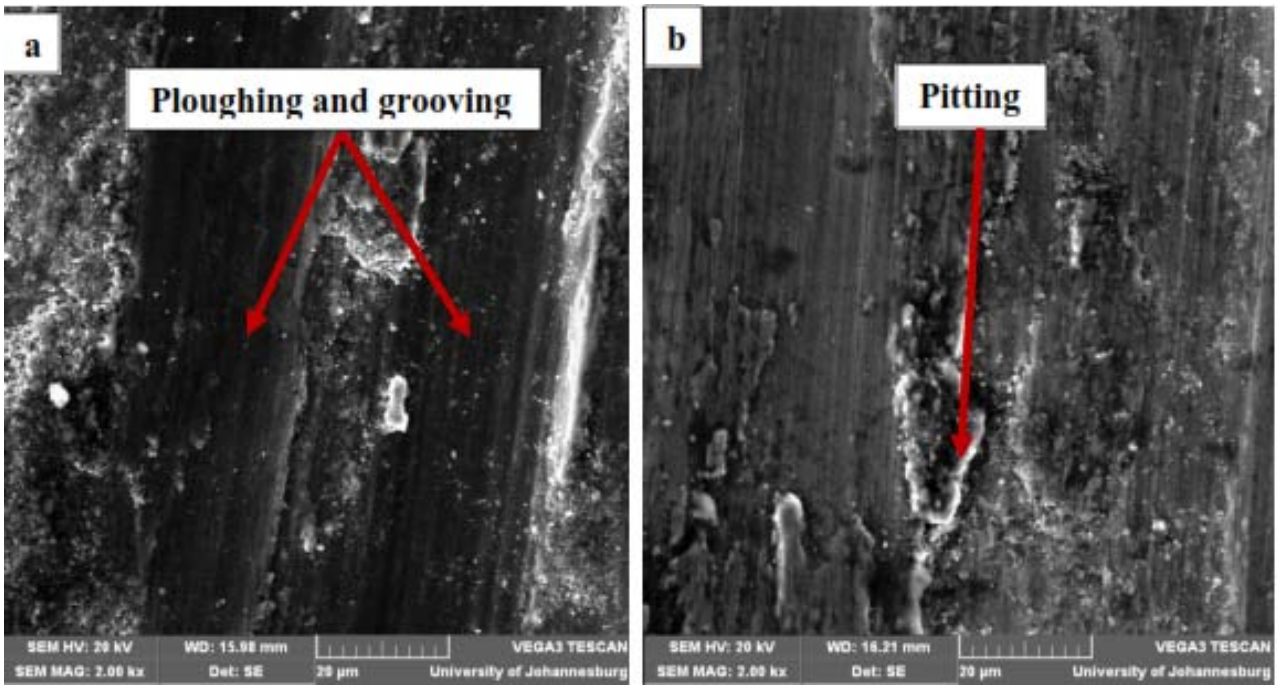

Figure 11

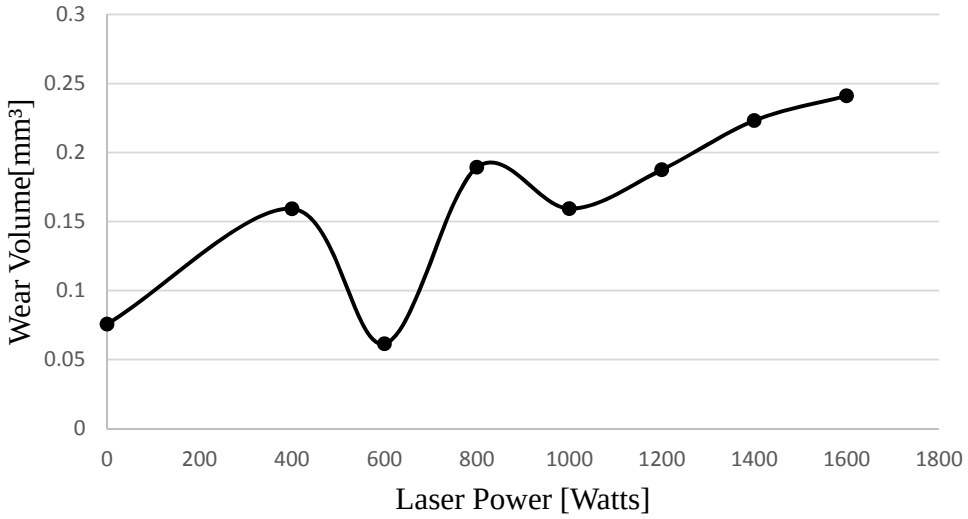
0.3
0.25
0.2
0.15
0.1
0.05
0
Wear Volume[mm³]
0
200
400
600
800
1000
1200
1400
1600
1800
Laser Power [Watts]

Figure 12

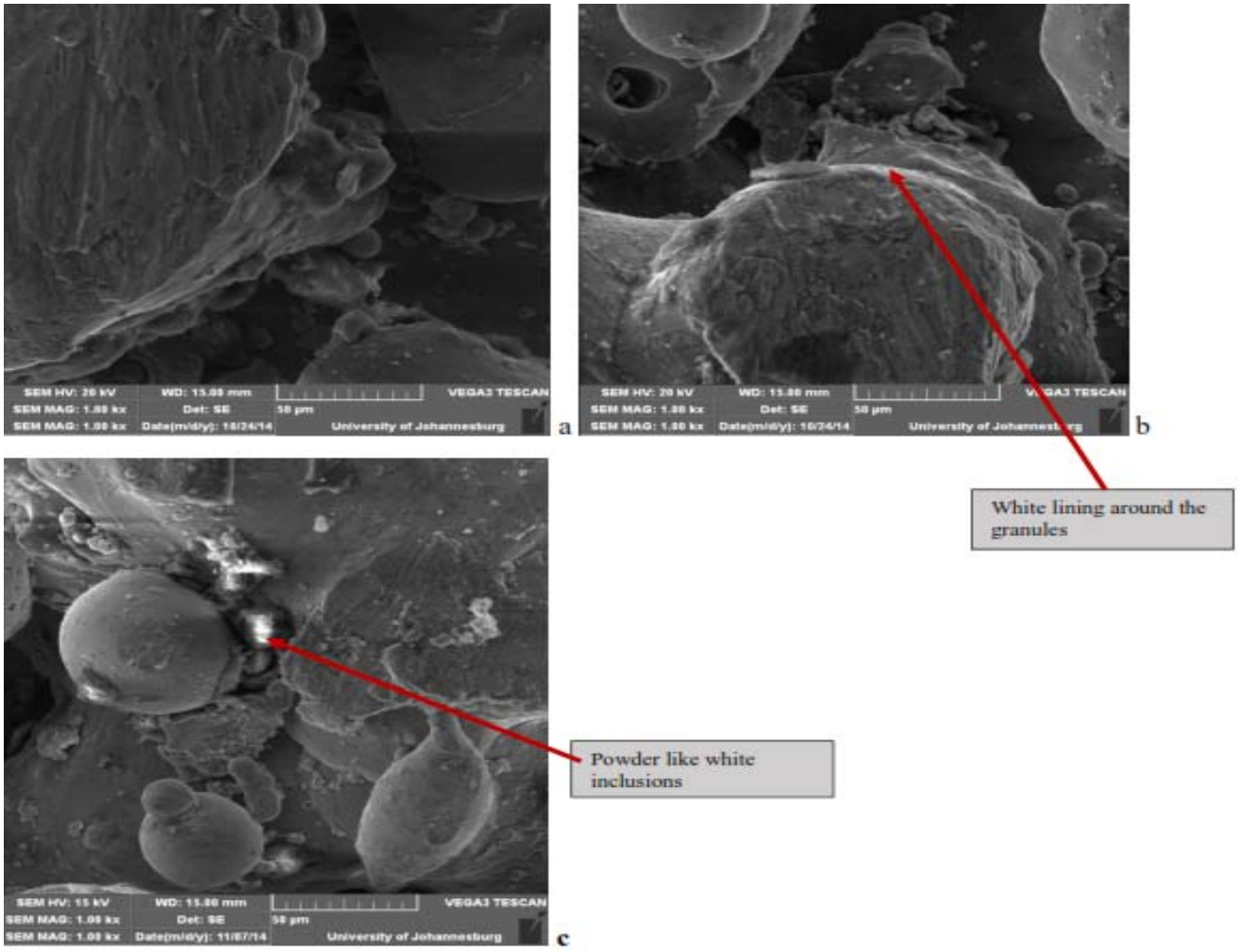

Figure 13

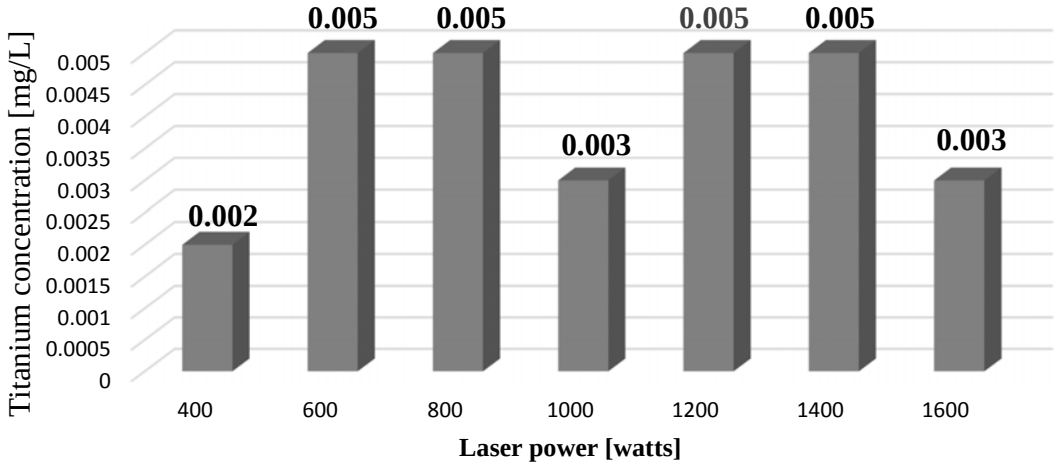

Figure 14